Inverse solution of ear-canal area function from reflectance

Daniel M. Rasetshwane[a] and Stephen T. Neely
Boys Town National Research Hospital, 555 North 30th Street, Omaha, Nebraska 68131

(Received 9 May 2011; revised 27 September 2011; accepted 30 September 2011)

A number of acoustical applications require the transformation of acoustical quantities, such as impedance and pressure that are measured at the entrance of the ear canal, to quantities at the eardrum. This transformation often requires knowledge of the shape of the ear canal. Previous attempts to measure ear-canal area functions were either invasive, non-reproducible, or could only measure the area function up to a point mid-way along the canal. A method to determine the area function of the ear canal from measurements of acoustic impedance at the entrance of the ear canal is described. The method is based on a solution to the inverse problem in which measurements of impedance are used to calculate reflectance, which is then used to determine the area function of the canal. The mean ear-canal area function determined using this method is similar to mean ear-canal area functions measured by other researchers using different techniques. The advantage of the proposed method over previous methods is that it is non- invasive, fast, and reproducible.
 [DOI: 10.1121/1.3654019]

PACS number(s): 43.64.Ha, 43.20.El, 43.20.Bi [BLM] Pages: 3873–3881

I. INTRODUCTION

The ear canal serves as an acoustical waveguide that links an external sound field with the eardrum. The transformation characteristic of sound pressure at this external field to sound pressure at the eardrum depends on the shape of the ear canal. The shape of the ear canal is important for prediction of sound pressure level (SPL) at the eardrum (Stinson and Lawton, 1989; Hudde, 1983a), determination of acoustic impedance at the eardrum (Zwislocki, 1957; Hudde, 1983b), characterization of ear-canal standing-wave ratio along the ear canal (Stinson, 1990), interpretation of physiological experiments (Khanna and Stinson, 1985), and extension of current audiometric techniques to high frequencies (Stevens, *et al*., 1987; Green *et al*., 1987). Knowledge of the ear-canal shape also is important for the development of high-frequency hearing aids (Egolf, 1980). Extending the high-frequency response of hearing aids is clinically relevant especially for children who may experience improvements in speech recognition with bandwidths that exceed those of currently available devices (e.g., Stelmachowicz *et al*., 2001). Fitting of completely-in-the-canal hearing aids may also benefit from knowledge of the canal shape. Knowledge of the shape of the ear canal also may be useful in assessing the status of the eardrum and the middle ear, as well as that of the canal itself.

This paper describes a method to determine the area function of the ear canal from measurements of acoustic impedance. The method is based on a solution to the inverse problem in which measurements of impedance, taken at the entrance of the ear canal, are used to calculate reflectance (e.g., Claerbout, 1985), which is then used to determine the ear-canal area function (cross-sectional area as a function of axial position). The method may provide a non-invasive and fast procedure for determining the shape of the ear canal that may be useful in the various applications outlined above.

Johansen (1975) used silicone-injection molds to determine the volume, as a function of axial distance, of human cadaver ear canals. The volume was determined by measuring the volume of liquid displaced by each 2 mm submersion of the ear-canal mold impression. Hudde (1983a) described a method to determine the shape of human ear canals from measurements of pressure made at three different locations along the canal. A broadband stimulus was used and measurements were taken at the entrance of the ear canal, near the eardrum and in between these two locations. The area function was obtained by minimizing a system of linear equations derived from Webster's horn equation (Webster, 1919). A straight center axis was assumed in the computation of the area functions. Results showed considerable variability in the area functions along the axis of the ear canal. Hudde (1983b) used the area functions as transformation characteristics to calculate the impedance and reflectance at the eardrum. However, Hudde's method has several limitations. The method fails in a conduit with unity reflections or if the middle measuring point lies exactly at the center of the other two. Additionally, area functions were only derived over the middle 18 mm of the ear canals, the placement of the probe required high precision, and discomfort was reported by subjects.

Stinson and Lawton (1989) determined the geometry of the ear canal of human cadavers using silicone-injection molds. The area function determined using a curved center axis that follows the curvature of the ear canal was different from that determined using a straight center axis. They observed considerable variability in ear-canal geometry among subjects. Stinson and Lawton showed that the SPL distribution in the ear canal depends on the geometry of the ear canal, especially for frequencies greater than 1 kHz. Stinson (1990) showed that accounting for the curvature of the ear canal allows for better fit of the ear-canal standing-wave

[a]Author to whom correspondence should be addressed. Electronic mail: daniel.rasetshwane@boystown.org

ratio (SWR) to assumed theoretical forms, especially at frequencies greater than 8 kHz. However, inter-subject variability was observed in the SWR.

Egolf *et al.* (1993) measured the area function of ear canals of human cadavers using a computer-assisted tomographic (CAT) scanner and silicone-injection molds method. They demonstrated good agreement between the two measurements. However, as with earlier studies, intersubject variability was observed. Comparison to the earlier studies of Stinson and Lawton (1989) showed only fair agreement, while comparison to Johansen (1975) showed good agreement. Although some agreement was demonstrated between the measurements of Johansen (1975), Stinson and Lawton (1989), and Egolf *et al.* (1993), the disadvantage of these three studies is that the techniques are not suitable for application to living humans. Also, the shape of the canal may change during rigor mortis.

Recently, Qi *et al.* (2006) used a computed tomography (CT) scan to acquire the geometry of the ear canal of a living newborn for the purpose of modeling ear-canal volume changes, and related tympanometric measures, caused by changes in ear-canal pressure. However, canal geometry was reported for only one subject. The high levels of radiation exposure and links to cancer (Brenner and Hall, 2007) have limited the use of this imaging technology for research purposes in living humans.

An inverse problem is a general framework that is used to convert measurements observed in an object into physical properties of that object. In acoustics, the inverse problem can be applied to determine physical properties such as the area function of an acoustical cavity from acoustical measurements such as impedance and pressure. The inverse problem has been used to determine the shape of the vocal tract from acoustic measurements at the lips (e.g., Schroeder, 1967; Mermelstein, 1967; and Sondhi and Gopinath, 1971). To our knowledge, there has been only one application of the inverse problem to determine the shape of the ear canal (Joswig, 1993). Joswig (1993) applied the method of Sondhi and Gopinath (1971) to determine the area functions of ear canals. Modifications were made to Sondhi and Gopinath's inverse solution, including a more numerically stable estimate of the impulse response, and a correction for the area function calculation to account for acoustical losses along the ear canal. Tests with a uniform tube and a conical horn to validate Joswig's algorithm produced accurate matches of area functions. However, applications to determine ear-canal area functions only produced a fair match to the results of Johansen (1975). Additional limitations of Joswig's method included problems encountered with the measurement equipment, and the fact that ear-canal lengths could only be measured up to a maximum length of 21 mm (this is shorter than the average ear-canal length of a human adult, e.g., 25.7 mm according to Johansen, 1975). The method of Hudde (1983a) may be interpreted as a form of an inverse solution since it determines area functions of the ear canal from measurements of pressure. However, Hudde's method has the limitations mentioned above.

In this paper, we formulated a solution to the inverse problem that begins with recasting of Webster's horn equation in terms of forward- and backward- traveling pressure waves. The wave variables are obtained through decomposition of the total acoustical pressure. An essential part of the solution to the inverse problem is a new definition of reflectance that is compatible with the solution and consistent with current definitions of reflectance. Compared to Hudde's method, the current method only requires a single measurement at the entrance of the ear canal. Compared to Joswig's method, our method can determine the area function of the entire ear-canal length. Recent results from theoretical analysis of infinite acoustic horns (exponential, parabolic, and conical) and from measurements made in uniform tubes suggest that the current inverse solution can accurately determine area functions (Rasetshwane and Neely, 2011). The mathematical basis for the inverse solution is presented in the Appendix. Further validation of the inverse solution is presented here by (1) application to measurements made in an ear-canal simulator with a known shape and (2) comparison to previous publications of average cross-sectional area function measurements in human ear canals.

II. METHODS

A. Subjects

A total of 24 subjects with ages ranging from 15 to 65 years participated in this study. Subjects were required to have audiometric thresholds of 10 dB HL or better (ANSI, 1996) for the octave and interoctave frequencies from 0.25 to 8 kHz. Middle-ear status was assessed using tympanometry with a 226 Hz probe tone. To qualify for inclusion, the subjects had to meet the following criteria: peak-compensated static admittance of 0.3 to 2.5 mmhos and tympanometric peak pressure between −100 and +50 daPa. Otoscopic examination was also completed as a way to further assess the ear-canal and middle-ear status. All subjects were recruited from a database of potential research subjects, which is maintained at Boys Town National Research Hospital (BTNRH). Subjects were paid for their participation. The study described in this article was conducted under an approved Institutional Review Board protocol. After obtaining informed consent, and audiometric, tympanometric and otoscopic assessments, data collection required less than 5 min per subject.

B. Measurement equipment

The measurement equipment is a custom system that consists of two identical sound sources and one probe microphone (see Fig. 1). The ER-10B+ microphone (Etymōtic Research, Elk Grove Village, IL) allows the attachment of two sound sources by means of thin plastic tubes. The sound sources were developed by Jon H. Siegel at Northwestern University. Each sound source was constructed from a commercially available tweeter (TW010F1, Audax, France) that had been modified to allow attachment of Teflon plastic tubing. One end of the tubing is attached to a plastic cone that is glued in front of the cone of the tweeter. The other end of the tubing is attached to the sound ports of an ER-10B+ probe. Rigid plastic tubing (length: 28 cm, outside diameter:

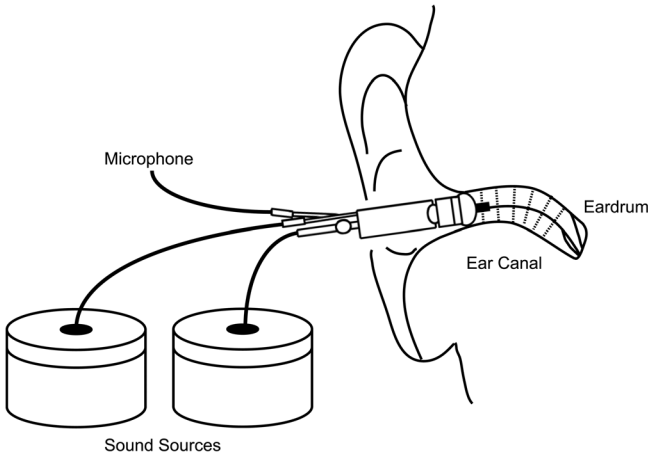

FIG. 1. Measurement equipment and general ear canal shape. Tweeters housed in lightweight steel cans are used as sound sources. The sound sources are connected to the sound ports of an ER-10B+ probe using Teflon plastic tubing. The tweeters were driven by a power amplifier that prevented overloading of the soundcard by the low-impedance speakers.

1.06 mm, inside diameter: 0.56 mm) reduces both propagation losses along the tube and acoustical cross-talk. Lightweight steel enclosures shield the tweeters from electromagnetic radiation to reduce electrical crosstalk. The tweeters were driven by a power amplifier (also designed at Northwestern University) that prevented overloading of the soundcard (Layla3G, Echo, Santa Barbara, CA) by the low-impedance speakers. The weight of the sound sources was supported by a swivel-mount microphone boom to allow placement in close proximity to the cavities (for calibration) and ear canal (for data collection). The two sound sources of the measurement system allow for a pair of measurements, made one at a time, for each probe placement. This sound-delivery system has a wider bandwidth, lower distortion and lower crosstalk compared to the ER-10C (Etymōtic Research), which combines two sound sources and a microphone (Neely and Siegel, 2011).

A wideband linear-swept frequency chirp signal, generated digitally at a sampling rate of 48 kHz, was used as the stimulus. The stimulus level (measured in the ear canal at the plane of the probe) was 90 dB SPL. Stimulus delivery and data collection were monitored using locally developed software (EMAV; Neely and Liu, 1994).

C. Calibration

The measurement system was calibrated prior to data collection to determine the Thévenin- equivalent source impedance and pressure (Allen, 1986; Keefe *et al*. 1992; Scheperle *et al*., 2008). Six uniform-diameter cavities of varying lengths were used as standard acoustic loads for determining Thévenin-equivalent source pressure and impedance. The cavities were constructed of brass tubing (8 mm i.d.). The lengths of the brass tubes were selected to produce six half-wave resonant peaks at approximately 2878, 3289, 4112, 4638, 5345, and 7401 Hz. A wideband linear-swept frequency chirp was used for Thévenin-equivalent source calibration. Thévenin-equivalent source parameters were determined for each sound source, separately.

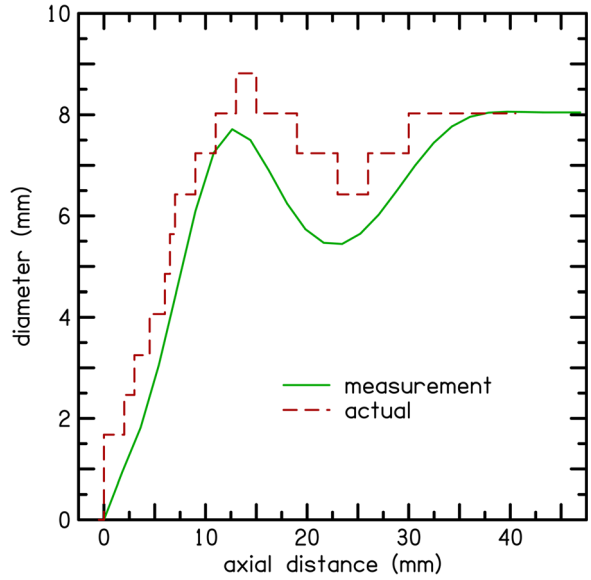

FIG. 2. (Color online) Ear canal simulator diameter inverse solution (solid line) obtained from the time-domain reflectance using the inverse solution. Dashed line shows the true diameter function for comparison.

D. Validation of the inverse solution

The inverse solution was implemented in MATLAB (MathWorks, Inc.) based on the mathematical description in the Appendix. To validate the inverse problem, measurements of impedance were made in an ear-canal simulator, converted to reflectance, and then the inverse solution was applied to generate area function. The ear-canal simulator was constructed using fifteen concentric segments of brass tubes with varying cross-sectional area. A stainless steel dowel was used to terminate the distal end. The segments were tightly glued together to establish an acoustical seal. A simple coupler was fashioned from a section of brass tubing with concentric diameter to allow convenient connection to the ER-10B+ probe and its foam tip. The diameter function $D(x)$ of the ear-canal simulator is shown in Fig. 2 (dashed line). The solid line in Fig. 2 shows $D(x)$ obtained using the inverse solution. There is good correspondence to actual diameter function, except for the slight underestimation of the diameter constriction at $x = 25$ mm and expansion at $x = 11$ mm. Area function can be obtained from diameter function using $A(x) = \pi(D(x)/2)^2$.

E. Estimation of ear-canal characteristic impedance

Measurements of acoustic load impedance Z_L were made in the 24 subjects who participated in this study. Data for three subjects were excluded from analysis because of measurement artifacts observed in the data that produced unrepeatable reflectance values when analyzed. Consequently, results from 21 out of 24 data sets are described in this paper.

The load impedance was then used to calculate reflectance

$$R(x,\omega) = \frac{Z_L(x,\omega) - Z_0(x)}{Z_L(x,\omega) + Z_0(x)}, \quad (1)$$

where Z_0 is the characteristic impedance (e.g., Claerbout, 1985). The characteristic impedance of the ear canal is

$$Z_0 = \frac{\rho c}{A(x)}, \tag{2}$$

where ρ is the density of air, c is the speed of sound, and $A(x)$ is the canal cross-sectional area at axial position x along the ear canal.

It is important to accurately estimate the characteristic impedance. Use of an incorrect area at the entrance of the ear canal can lead to errors in the calculation of reflectance. For example, assuming that the area is equal to that of the calibration brass tube and using the characteristic impedance of the brass tube as the characteristic impedance at the entrance of the ear canal. The characteristic impedance for the reflectance calculation was determined by the following iterative procedure that estimates the "surge" component of the load impedance.

(1) The initial estimate of Z_0 was calculated by Eq. (2) as the characteristic impedance of the brass tube used for calibration (81.55 cgs acoustic ohms at 25 °C).
(2) The time-domain reflectance (TDR) at $t=0$ was calculated by Eq. (1) using the current estimate of Z_0. A frequency-domain window, described later, was applied in the computation of reflectance to eliminate ringing in the TDR.
(3) Z_0 was adjusted using the calculated TDR in a way that reduces the TDR at $t=0$.
(4) Steps 2 and 3 are repeated until the value of Z_0 converge to a single value.

The convergence of the characteristic impedance is demonstrated in Fig. 3, where different symbols are used to represent data from each of the 21 subjects and lines with the identical symbols represent the two sound sources for the same subject. Convergence is usually attained before the eighth iteration (indicated with a dashed vertical line).

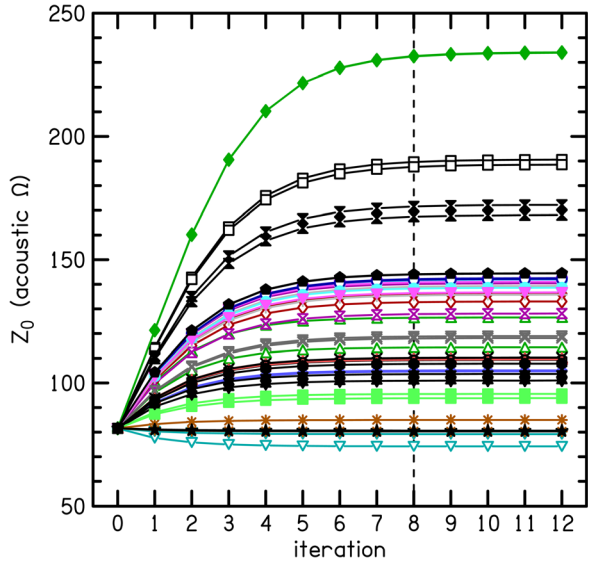

FIG. 3. (Color online) Convergence of the estimate of characteristic impedance. Lines with the same symbol represent the two sound sources for the same subject. Convergence is usually attained before the eighth iteration (indicated with a dashed vertical line).

F. Computation of ear-canal area function

Frequency-domain reflectance was calculated from the measured load impedance and the estimate of the characteristic impedance using Eq. (1). TDR was calculated as the inverse Fourier transform of the frequency-domain reflectance and the inverse-solution method was applied to obtain an area function $A(x)$ from the TDR. The inverse solution assumes a sound propagation path that is perpendicular to the plane of the emission probe, whereas the ear canal has curvature, as shown in Fig. 1. The effect of this assumption will be discussed later.

Three signal-processing techniques were used to mitigate the effect of the finite sampling rate and to reduce the impact of measurement error. Preliminary analyses indicated that these signal processing steps improved the inverse solution results.

(1) Sampling-rate upconversion—the sampling rate of the data was effectively increased by a factor of 4 (up to 192 kHz) by zero padding the spectrum to provide adequate sampling density for the inverse solution.
(2) Frequency-domain window—a Blackman window with a 17-kHz half-width was applied in the frequency-domain to reduce contributions from higher frequencies (where the measurement was less reliable) and to eliminate ringing in the time domain.
(3) Time-reversed addition—the TDR for $t<0$ was time-reversed and added to the reflectance for $t>0$ to remove a signal-processing artifact observed in the data.

Techniques 1 and 2 were applied prior to the calculations of the TDR and the application of the inverse solution to generate area function. This produced a TDR that was smooth and improved the convergence of the inverse solution. A Blackman window was used because it has less sideband leakage than equivalent length Hamming and Hanning windows, which, in this case, reduces spread in the TDR. Time-reversed addition was observed to improve cross-channel similarity between the two sound sources.

III. RESULTS

The range of the final estimate of characteristic impedance in Fig. 3 is due to differences in the ear-canal diameters of the subjects at the plane of the probe. The mean and standard deviation for this diameter are 6.51 and 0.89 mm. The corresponding mean values for cross-sectional area and characteristic impedance are 33.3 mm^2 and 123 cgs acoustic ohms, respectively. We believe that spatial separation of the sound ports (1 mm) of the ER-10B + contributed to the differences observed in measurements from the two sources because the sound waves emanating from the two sources followed slightly different propagation paths.

The mean frequency-domain reflectance for the 21 subjects is shown in Fig. 4. The top panel shows the reflectance magnitude in decibels and the lower panel shows the group delay, defined as

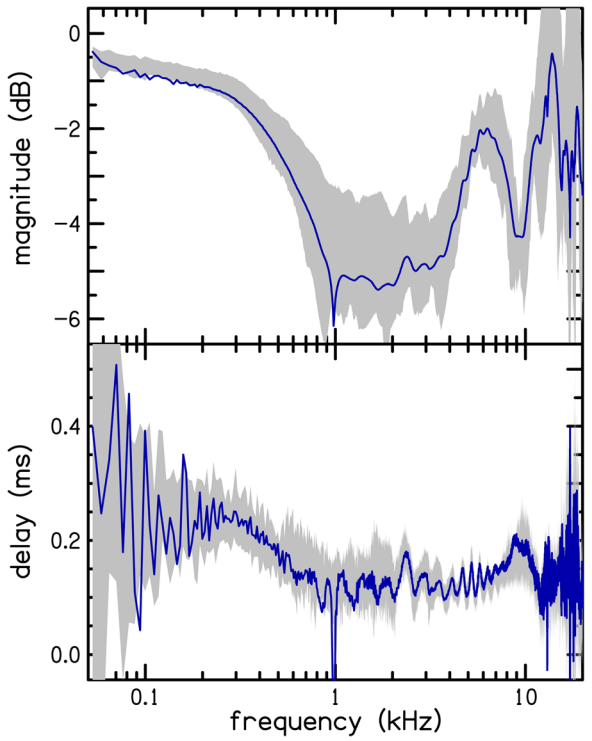

FIG. 4. (Color online) Mean ear canal frequency-domain reflectance. The shaded region indicates data between the 25th and 75th percentiles.

$$\tau(\omega) = -\frac{\partial R(0,\omega)}{\partial \omega} \tag{3}$$

in ms. The shaded region defines the range of data between the 25th and 75th percentiles. The reflectance magnitude is approximately 0 dB at low frequencies (less than 0.2 kHz), decreases to a minimum value at a frequency between 1 and 3.5 kHz, and then increases at higher frequencies, where reflectance again approaches 0 dB. The frequencies of the higher-frequency peaks of approximately 6.5 and 14 kHz are within subject variability of the 8 and 11 kHz frequencies observed by Stinson (1990). The high value of the reflectance magnitude at low and high frequencies indicates that most of the sound at these frequencies is reflected by the eardrum and the walls of the ear canal. The group delay shows less variability than the reflectance magnitude in the frequency range 0.2–10 kHz. The group delay is also positive in this frequency range. Outside this range, the group delay oscillates. The differences in the reflectances may be due to differences in the curvature of the individual ear canals and differences in the direction of insertion of the measurement probe.

Time-domain reflectance (TDR) was obtained from frequency-domain reflectance by applying an inverse Fourier transform after application of the signal-processing techniques discussed above. Figure 5 shows the average TDR for the 21 subjects. The reflectances of the individual subjects were translated in time so that the latency of the largest peak was equal to the average latency for the peak (0.14 ms). The shaded region defines the interquartile range of the data. There is less intersubject variability in the TDR compared to the frequency-domain reflectance, due to the signal

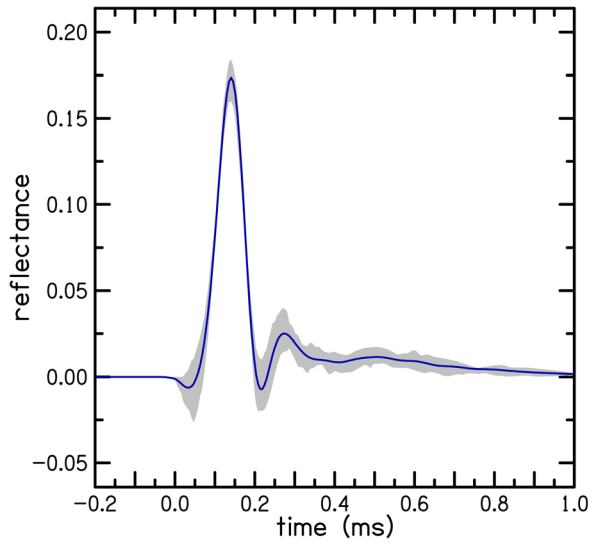

FIG. 5. (Color online) Mean ear canal time-domain reflectances (TDR). The TDR of individual subjects were translated in time so that the latency of the largest peak equals the average latency (0.14 ms). Shaded region indicates data between 25th and 75th percentiles.

processing described in the Methods section. The reflectances are zero-valued for $t \leq 0$ as a consequence of the time-reversed addition (also described in Sec. II). The largest peak of the TDR has a value in the range of 0.14 to 0.23, with a mean peak value of 0.18. This peak has latency in the range 0.08 to 0.17 ms, with a mean latency of 0.14 ms, which corresponds to the round-trip propagation time for sound to travel from the probe to the eardrum and back to the probe. The cumulative distribution of this latency is shown in Fig. 6 for the 21 subjects. The median latency, indicated by the dotted dashed line, is 0.14 ms. The median latency is the same as the mean latency (0.14 ms), which is the round-trip travel time for a distance of 24 mm.

Results of the application of the inverse solution to generate ear-canal area functions $A(x)$ from the TDR are shown in Fig. 7. Specifically, Fig. 7 shows the mean area function and the shaded region that indicates data between the 25th and 75th percentiles. Area functions for individual subjects are shown in Fig. 8 and discussed later. The position of the eardrum corresponds to $x = 0$ mm. The position of the eardrum and the canal lengths were determined using sound propagation delay from the plane of the probe to the eardrum measured using the autocorrelation of the time-domain pressure measurement. The canal lengths vary from 14.20 mm to 29.36 mm, with a mean length of 24.08 mm. Since the ear canals are of different lengths, the number of samples included in the computation of the mean area function at location x varies depending on the number of samples available. For location $x < 14.20$ mm (lower limit of length), all of the ear canals are included. However for $x = 29.36$ mm, only one ear canal is included.

The area function determined using the inverse solution is non-zero beyond the eardrum due to the spreading of the TDR caused by the use of the frequency-domain Blackman window for smoothing the reflectance. Also, the non-zero value of TDR beyond the first large peak (corresponding to

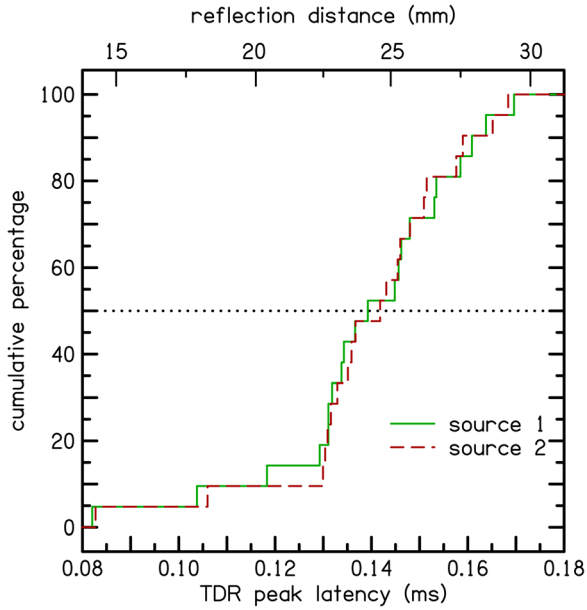

FIG. 6. (Color online) Cumulative distribution of time-domain reflectance (TDR) peak latency for the two sound sources. The TDR peak latency represent the round-trip travel time to the point of reflection, the eardrum. The median latency, indicated by the horizontal dotted line, is 0.14 ms. The median latency is the same as the mean latency (0.14 ms), and corresponds to a reflection distance of 24 mm.

the eardrum), due to acoustic energy transmitted through the eardrum, causes the inverse solution to produce a non-zero area function beyond the eardrum. The position where $A(x) = 0$ corresponds to the time instant when the value of the TDR is zero.

There is more variability in the ear-canal area functions than was observed in both the frequency- and time-domain

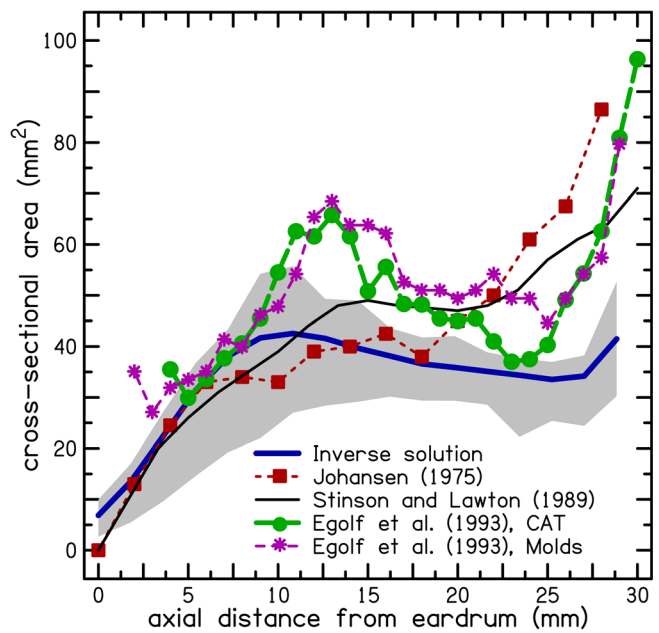

FIG. 7. (Color online) Mean ear-canal area function obtained from inverse solution. Shaded region indicates data between the 25th and 75th percentiles. The location of the eardrum is $x = 0$. Comparison is made to data from Johansen (1975), Stinson and Lawton (1989), and Egolf *et al.* (1993). The mean ear-canal area function of the current study is similar to the area functions reported by the earlier studies.

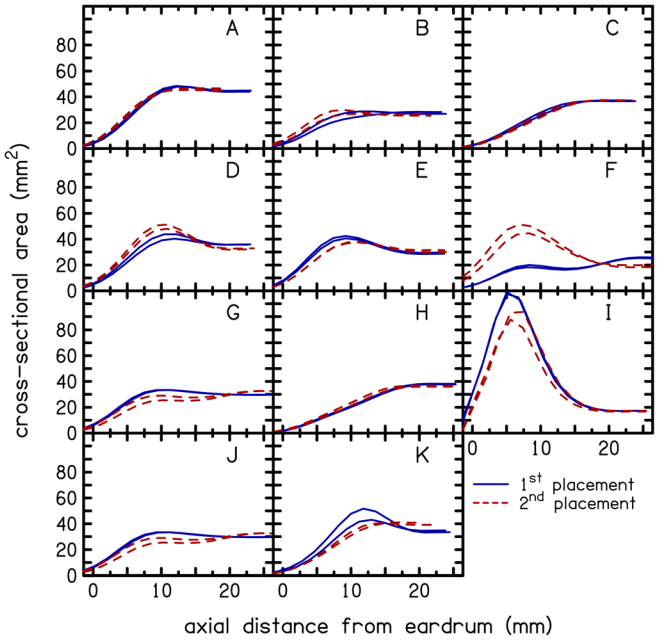

FIG. 8. (Color online) Reproducibility of ear-canal shape by inverse solution. Ear-canal area functions for eleven subjects are shown for two different probe placements. In each panel, lines with the same line style compare measurements from the two sound sources. The ear-canal area function from the first probe placement is similar to the area function from the second probe placement, except for subject F. The area function generated by the inverse solution is reproducible.

reflectances. This larger variability is presumably due to hypersensitivity of the inverse solution to small changes in TDR. Expansion of the area function is associated with negative reflectance observed in the time-domain. For example, negative TDR between $t = 0$ and the positive peak (see Fig. 5) causes the area function to increase between the plane of the probe and the eardrum.

For comparison, Fig. 7 also includes the mean area function reported by Johansen (1975), Stinson and Lawton (1989), and Egolf *et al.* (1993). Johansen's area function was obtained by dividing the volume function by unit length. For Egolf *et al.* (1993), area functions are plotted for both the CAT-scan method and the injection-mold method. The average ear-canal area function of our study is similar to the area functions reported by these earlier studies. The average area function should be regarded as suggestive since intersubject variability was observed in the data.

The volume of the ear canal was obtained from $A(x)$ by numerical integration with respect to axial distance from the eardrum to the location of the probe, i.e.,

$$V = \int A(x)dx, \tag{4}$$

The volume of the ear canals of the 21 subjects varies from 372 to 1 464 mm^3, with a mean volume of 843 mm^3.

IV. DISCUSSION

The mean ear-canal area function obtained using the inverse solution shows agreement with the area functions reported previously by Johansen (1975), Stinson and Lawton

(1989), and Egolf *et al.* (1993). There is also agreement in mean ear-canal volume and length. The mean ear-canal volume of 843 mm^3 obtained in this study is lower than the mean volumes reported by Stinson and Lawton (1989) (1271 mm^3) and Egolf *et al.* (1993) (1211 mm^3 with CAT-scan method and 1290 mm^3 with the injection-mold method). The mean ear-canal length of 24 mm obtained in this study is also shorter than the mean length reported by Stinson and Lawton (1989) (30 mm). However, the measurements of Stinson and Lawton (1989) and Egolf *et al.* (1993) included part of the concha, while our measurements excluded the concha plus the space taken by the foam tip of the measurement probe. The discrepancy between the inverse solution and previous measurements for axial distance $x > 20$ mm is also partly due to biased representation of the subject population. When the axial distance is large, subjects with short ear canals are excluded from the mean and range calculations. Comparison to results of Joswig (1993) is not possible since he did not report mean area functions. However, we would contend that the current method performs better than that of Joswig because his reported subject ear-canal area functions did not include the first 5 mm from the eardrum and had a maximum range of 21 mm.

To evaluate whether the area functions generated by the inverse solution are reproducible, two sets of measurements were collected in some subjects with the measurement probe removed from and then re-inserted back into the subject's ear between the two sets of measurements. If the area function is reproducible, the area function from the two measurements with different probe placements would be similar. The only difference should be due to differences in the probe insertion depth. The measurements for this evaluation were collected on the last eleven of the 21 subjects. Figure 8 shows ear-canal area functions for this evaluation. In each panel, lines with the same line style compare measurements from the two sound sources. For ten of the eleven subjects, the ear-canal area function from the first probe placement is similar to the area function from the second probe placement. The area function for one subject (subject F) was not well reproduced. Based on these results, we conclude that the area function generated by the inverse solution is reproducible in individual ears. Figure 8 also demonstrates considerable variability of ear-canal shape across subjects. Because ear-canal shape influences reflectance measurements, its variability is relevant to the clinical interpretation of ear-canal reflectance.

Although we have no direct measurements to verify our ear-canal area functions, the existence of well-behaved inverse solutions supports the validity of the reflectance measurement, which requires having a reliable estimate of characteristic impedance. Imaging technologies may provide a means to verify the area functions. However, radiation exposure associated with the CT scan has limited its use in research involving living humans. Other imaging technologies with lower radiation levels, such as magnetic resonance imaging, are not readily accessible due to high costs. Recently available laser scanning technologies for hearing-aid fitting (e.g., Sullivan, 2007) do not scan the ear canal itself, but an impression of the ear canal that is made from a silicone-type injection mold. This mold is typically injected into the ear canal only as deep as mid-way along the canal.

The proposed inverse solution is sensitive both to analysis parameters and to measurement errors. It is particularly sensitive to the half-width of the Blackman window used for frequency-domain smoothing. Care was taken in parameter selection to minimize errors in the computed area functions. Another issue with the inverse solution is that it has a limited spatial resolution ($\sim$7.2 mm) which produces area functions that are smooth and do not capture rapid changes in ear-canal shape. Future improvements to the inverse solution may allow for improved spatial resolution by extending reflectance measurements to higher frequencies. Our assumption of a straight center axis for the ear canal may have led to an under-estimation of the canal length and volume (Stinson and Lawton, 1989). Modeling for the curvature, although sophisticated, may improve our estimates of area functions.

In the inverse solution, type-I reflectance (see the Appendix) adequately describes wave propagation at the entrance of the ear canal, $x = 0$. However, type-II reflectance is needed to describe the two-sided wave propagation at $x > 0$ where reflection of reverse waves contributes to forward waves. The range of frequencies (50 Hz to 20 kHz) in the reflectance measurements of Fig. 4 is wider than previously reported measurements for living humans. Most studies typically report measurements only up to 10 kHz. We attribute this wide range of frequencies to the wider bandwidth, lower distortion and lower crosstalk of our measurement equipment, which helped to avoid the measurement problems reported by Joswig (1993).

The procedure described for estimating characteristic impedance may offer a way to improve measurements of reflectance when the actual cross-sectional area at the entrance of the ear canal is unknown. A possible clinical benefit of the inverse-solution may be that it validates the estimate of characteristic impedance. Correct estimation of the characteristic impedance is essential in other clinical applications such as forward-pressure level (FPL) calibration (Scheperle *et al*, 2008) and the proposed estimation method was shown to reduce FPL errors by the same amount as calculating characteristic impedance from known tube areas (Scheperle *et al*., 2011).

The peak value of TDR for the ear canals is between 0.14 and 0.23. This peak may indicate mobility of the eardrum. The second smaller peak occurring about 0.13 ms after the first is close to the middle-ear transmission delay of 0.12 ms (see Fig. 5, Puria, 2003), and we suggest indicates mobility of the stapes. The peak value of the TDR for brass uniform tubes is between 0.26 and 0.28 (Rasetshwane and Neely, 2011). This peak value was shown to be independent of the length (Rasetshwane and Neely, 2011) and diameter (Scheperle *et al*., 2011) of the tube. The difference in peak values implies that the peak value of TDR can distinguish tubes from ear canals. We interpret the difference in peak value of TDR to indicate that the distal end of the tubes is more rigid than the typical eardrum. These results add support for the potential use of reflectance for the evaluation of the 'rigidity' of the eardrum. In turn, this could have clinical implications for assessing middle-ear function.

V. CONCLUSION

A method to determine ear-canal area functions from reflectance is described. The area functions generated by the method are similar to area functions obtained by others using different techniques. The proposed method may offer a non-invasive and relatively fast procedure for determining the shape of the ear canal that is also reproducible. Although inadequate spatial resolution and excessive sensitivity to analysis parameters may limit the accuracy of the method, ear-canal shape estimates could enable improved characterization of various properties of the external and middle ear.

ACKNOWLEDGMENTS

Research was supported by grants from NIH (Grants Nos. R01 DC8318 and P30 DC4662). We would like to thank Cori Birkholz, Alyson Truog, and Judy Kopun for their help in recruiting subjects and making measurements. We would like to thank Jonathan H. Siegel for providing us with the sound-delivery equipment. Finally, we thank Brenda Lonsbury-Martin, two anonymous reviewers, and Michael Gorga for helpful suggestions on earlier versions of this manuscript.

APPENDIX: INVERSE SOLUTION FOR THE HORN EQUATION

Under the assumption of lossless plane-wave propagation in a tube of variable cross-sectional area $A(x)$, the equations relating acoustic pressure $p(x,t)$ and volume velocity $u(x,t)$ are

$$\partial_x p = -\frac{\rho}{A(x)}\partial_t u, \tag{A1}$$

$$\partial_x u = -\frac{A(x)}{\rho c^2}\partial_t p, \tag{A2}$$

where ρ is the density of air and c is the speed of sound (Webster, 1919). This relation is known as the "horn equation." Typical solutions of the horn equation evaluate $p(x,t)$ and $u(x,t)$ given $p(x,0)$, $u(x,0)$, and $A(x)$. The inverse solution we seek evaluates $A(x)$ given $A(0)$, $p(0,t)$, and $u(0,t)$.

The first step in the derivation of our inverse solution is to decompose $p(x,t)$ into wave variables $p_+(x,t)$ and $p_-(x,t)$ that satisfy two expected properties: (1) superposition and (2) causality. The superposition requirement is simply that their sum is the total pressure:

$$p(x,t) = p_+(x,t) + p_-(x,t). \tag{A3}$$

The causality requirement is that the deconvolution of $p_-(x,t)$ by $p_+(x,t)$ is zero for $t<0$ for all values of x. This deconvolution is more easily expressed in the frequency domain as a transfer function

$$R(x,\omega) = \frac{P_-(x,\omega)}{P_+(x,\omega)}, \tag{A4}$$

where $P_+(x,\omega)$ and $P_-(x,\omega)$ are the Fourier transforms of $p_+(x,t)$ and $p_-(x,t)$ and $R(x,\omega)$ is called "reflectance."

In a uniform tube, $p_+(x,t)$ and $p_-(x,t)$ are not coupled to each other by the horn equation. In this case, the ratio of $p_+(x,t)$ and $p_-(x,t)$ is usually called the "reflection coefficient" and may be expressed as

$$R_I(x,\omega) = \frac{Y_0(x) - Y_r(x,\omega)}{Y_0(x) + Y_r(x,\omega)}, \tag{A5}$$

where the *radiation admittance* is defined as

$$Y_r(x,\omega) \equiv \frac{U(x,\omega)}{P(x,\omega)}, \tag{A6}$$

(e.g., Keefe *et al.*, 1992). We refer to Eq. (A5) as type-I reflectance. In Eq. (A6), $P(x,\omega)$ and $U(x,\omega)$ are Fourier transforms of $p(x,t)$ and $u(x,t)$. The radiation and surge admittances may be determined experimentally from measurements of $P(x,\omega)$ and $U(x,\omega)$. In terms of the general horn equation, $Y_0(x) = A(x)/\rho c$. In a uniform tube, $Y_0 = A_0/\rho c$ is a constant, independent of x.

In a non-uniform acoustic horn, an inverse Fourier transform of the right hand side of Eq. (A5) may become non-zero at $t=0$ due to the reactive component of Y_r. In order to restore strict causality, we introduce the following expression as our definition of reflectance:

$$R_{II}(x,\omega) \equiv \frac{Y_0(x) - [Y_r(x,\omega) - Y_s(x,\omega)]}{Y_0(x) + [Y_r(x,\omega) - Y_s(x,\omega)]}, \tag{A7}$$

where Y_s is subtracted from Y_r to ensure that the initial value of reflectance is zero in the time- domain. We refer to Eq. (A7) as type-II reflectance. The quantity Y_s is called the step *admittance* because of its time-domain properties and is defined by the following expression:

$$Y_s(x,\omega) \equiv Y_0(x)\frac{c}{i\omega}B(x), \tag{A8}$$

where $B(x)$ is an undetermined variable that represents the inertial component of the radiation admittance at high frequencies for $x>0$. However, at $x=0$, we set $Y_s = B = 0$. So, at $x=0$, Eq. (A7), type-II reflectance, reduces to Eq. (A5), type-I reflectance.

The following definitions of $P_+(x,\omega)$ and $P_-(x,\omega)$ are derived by substituting for Y_s and Y_r in Eq. (A7), then comparing the result with the definition of reflectance in Eq. (A4):

$$P_+(x,\omega) = \frac{1}{2}\left\{P(x,\omega)\left[1 - \frac{c}{i\omega}B(x)\right] + \frac{U(x,\omega)}{Y_0(x)}\right\}, \tag{A9}$$

$$P_-(x,\omega) = \frac{1}{2}\left\{P(x,\omega)\left[1 + \frac{c}{i\omega}B(x)\right] - \frac{U(x,\omega)}{Y_0(x)}\right\}. \tag{A10}$$

The corresponding wave variables in the time domain are described by the following equations:

$$P_+(x,t) = \frac{1}{2}\left\{P(x,t) + \left[\frac{u(x,t)}{Y_0(x)} - cB(x)\int_0^t p(x,t)dt\right]\right\}, \tag{A11}$$

$$P_-(x,t) = \frac{1}{2}\left\{P(x,t) - \left[\frac{u(x,t)}{Y_0(x)} - cB(x)\int_0^t p(x,t)dt\right]\right\}. \tag{A12}$$

Solving Eqs. (A11) and (A12) for $p(x, t)$ and $u(x, t)$ and substituting into Eqs. (A1) and (A2) yields expressions for Webster's horn equation in terms of our wave variables:

$$\left[\partial_x + \frac{1}{c}\partial_t\right]P_+ = -\frac{1}{2}Bp - \left[\left(\varepsilon - \frac{1}{2}B\right)\frac{u}{Y_0} + \eta\int_0^t pdt\right], \tag{A13}$$

$$\left[\partial_x - \frac{1}{c}\partial_t\right]P_- = -\frac{1}{2}Bp + \left[\left(\varepsilon - \frac{1}{2}B\right)\frac{u}{Y_0} + \eta\int_0^t pdt\right], \tag{A14}$$

where

$$\varepsilon(x) \equiv \frac{1}{2}\frac{d}{dx}\ln A(x), \tag{A15}$$

is the logarithmic gradient of the horn diameter and

$$\eta(x) \equiv \frac{c}{2}\frac{d}{dx}B(x). \tag{A16}$$

When $p_+(0,t)$ is a Kronecker delta function, i.e., $p_+(0,t) = 1$ at $t = 0$ and $p_+(0,t) = 0$ for $t \neq 0$, then $p_-(0,t)$ is, by definition, the time-domain reflectance. This makes knowledge of the time-domain reflectance at $x = 0$ sufficient to calculate $A(x)$ and $B(x)$. Numerical integration for $x > 0$ of a finite-difference approximation of Eqs. (A13) and (A14) evaluates $A(x)$ and $B(x)$ by requiring these variables to satisfy the wave-front boundary condition at $x = ct$ (i.e., reflected pressure vanishes to zero). Thus, by evaluating $A(x)$, numerical integration of Eqs. (A13) and (A14) provides the desired inverse solution.

Allen, J. B. (**1986**). "Measurement of eardrum acoustic impedance," in *Peripheral Auditory Mechanisms*, edited by J. B. Allen, J. L. Hall, A. Hubbard, S. T. Neely, and A. Tubis (Springer-Verlag, New York), pp. 44–51.

American National Standards Institute (**1996**). "Specifications for audiometers," ANSI S3.6-1996, New York.

Claerbout, J. (**1985**). *Imaging the Earth's Interior* (Blackwell Scientific, Palo Alto), pp 287–289.

Egolf, D. P., Nelson, D. K., Howell, H. C., III, and Larson, V. D. (**1993**). "Quantifying ear canal geometry with multiple computer-assisted tomographic scans," J. Acoust. Soc. Am. **93**, 2809–2819

Egolf, D. P. (**1980**). "Techniques for modeling the hearing aid receiver and associated tubing," in *Acoustical Factors Affecting Hearing Aid Performance*, edited by G.A. Studebaker and I. Hochberg (University Park, Baltimore), pp. 297–319.

Green, D. M., Kidd, G., Jr., and Stevens, K. N. (**1987**). "High-frequency audiometric assessment of a young adult population," J. Acoust. Soc. Am. **81**, 485–494.

Hudde, H. (**1983a**). "Estimation of the area function of human ear canals by sound pressure measurements," J. Acoust. Soc. Am. **73**, 24–31.

Hudde, H. (**1983b**). "Measurement of the eardrum impedance of human ear," J. Acoust. Soc. Am. **73**, 242–247.

Johansen, P. A. (**1975**). "Measurement of the human ear canal," Acustica **33**, 349–351.

Joswig, M. (**1993**). "Impulse response measurement of individual ear canals and impedance at the eardrum in man," Acustica **77**, 270–282.

Keefe, D. H., Ling, R., and Bulen, J. C. (**1992**). "Method to measure acoustic impedance and reflection coefficient," J. Acoust. Soc. Am. **91**, 470–485.

Khanna, S. M., and Stinson, M. R. (**1985**). "Specification of the acoustical input to the ear at high frequencies," J. Acoust. Soc. Am. **77**, 577–589.

Mermelstein, P. (**1967**). "Determination of the vocal-tract shape from measured formant frequencies," J. Acoust. Soc. Am. **41**, 1283–1294.

Neely, S. T., and Liu, Z. (**1994**). "EMAV: Otoacoustic emission averager," Technical Memo No. 17 (Boys Town National Research Hospital, Omaha, NE).

Neely, S. T., and Siegel, J. H. (**2011**). "Comparison of sound sources for ear canal measurements," poster presented at the 34th Annual Midwinter Research Meeting of the Association for Research in Otolaryngology, Baltimore, MD.

Puria, S. (**2003**). "Measurements of human middle ear forward and reverse acoustics: Implications for otoacoustic emissions," J. Acoust. Soc. Am. **113**, 2773–2789.

Qi, L., Liu, H., Lutfy, J., Funnell, W. R. J., and Daniel, S. J. (**2006**). "A nonlinear finite-element model of the newborn ear canal," J. Acoust. Soc. Am. **120**, 3789–3798.

Rasetshwane, D. M., and Neely, S. T. (**2011**). "Inverse solution of ear canal shape from reflectance," poster presented at the (2011) American Auditory Society Scientific and Technology Meeting, Scottsdale, AZ.

Scheperle, R. A., Neely, S. T., Kopun, J. G., and Gorga, M. P. (**2008**). "Influence of in situ, sound-level calibration on distortion-product otoacoustic emission variability," J. Acoust. Soc. Am. **124**, 288–300.

Scheperle, R. A., Goodman, S. S., and Neely, S. T. (**2011**). "Further assessment of forward pressure level for *in situ* calibration," J. Acoust. Soc. Am. 130, 3882–3892.

Schroeder, M. R. (**1967**). "Determination of the geometry of the human vocal tract by acoustic measurements," J. Acoust. Soc. Am. **41**, 1002–1010.

Sondhi, M. M., and Gopinath, B. (**1971**). "Determination of vocal-tract shape from impulse response at the lips," J. Acoust. Soc. Am. **49**, 1867–1873.

Stelmachowicz, P. G., Pittman, A. L., Hoover, B. M., and Lewis, D. E. (**2001**). "Effect of stimulus bandwidth on the perception of/s/in normal- and hearing-impaired children and adults," J. Acoust. Soc. Am. **110**, 2183–2190.

Stevens, K. N., Berkovitz, R., Kidd, G., Jr., and Green, D. M. (**1987**). "Calibration of ear canals for audiometry at high frequencies," J. Acoust. Soc. Am. **81**, 470–484.

Stinson, M. R., and Lawton, B. W. (**1989**). "Specification of the geometry of the human ear canal for the prediction of sound-pressure level distribution," J. Acoust. Soc. Am. **85**, 2492–2503.

Stinson, M. R. (**1990**). "Revision of estimation of acoustic energy reflectance at the human eardrum," J. Acoust. Soc. Am. **88**, 1773–1778.

Sullivan, R. F. (**2007**). "Scan/print vs. invest/pour shell-making technologies for CIC hearing aid fittings," Hearing J. **60**, 21–28.

Webster, A. G. (**1919**). "Acoustical impedance, and the theory of horns and of the phonograph," Proc. Natl. Acad. Sci. **5**, 275–282.

Zwislocki, J. (**1957**). "Some measurements of the impedance at the eardrum," J. Acoust. Soc Am. **29**, 349–356.